

Measurement Notes

Note 53

Design and Fabrication of an Ultra-Wideband High-Power Zipper Balun and Antenna

Everett G. Farr
Farr Research, Inc.

Gary D. Sower, Lanney M. Atchley, and Donald E. Ellibee
EG&G MSI

January 1998

Abstract

We have designed, built and tested a coaxial zipper that can be used at high voltages. This device is designed to convert the signal from a single-ended (unbalanced coaxial) high-voltage output of Ultra-Wideband sources to a balanced configuration that can be radiated by a TEM horn. A variety of low voltage measurements were performed, including TDR and field measurements. The field at large distances was estimated from the measured data.

I. Introduction

We consider here the design and measurement of an Ultra-Wideband (UWB) zipper balun at high voltage. This work is an implementation of the design principles first outlined in [1]. Previously, low-voltage measurements on a scale model were provided in [2].

The need for high-voltage baluns is driven by the fact that many UWB sources have a coaxial, or single-ended output, but many antennas, such as TEM horns, require a balanced source. Thus, some sort of matching device or balun is necessary between the source and antenna. The task is made more difficult by two opposing factors that determine the size of the balun. The high voltages push the balun to larger sizes, in order to avoid dielectric breakdown. On the other hand, the fast risetimes push the balun to smaller sizes, in order to preserve bandwidth. Thus, a compromise in size is necessary in order to trade off device voltage and bandwidth.

We begin with a summary of the design principles and a description of the device. Next, we provide low voltage measurements of the device in air, with no TEM horn or lens attached. Finally, we provide measurements of the balun at low voltages in oil, with the TEM horn, lens, and oil box attached.

Let us start now with the design principles.

II. Zipper Design

We begin by looking at the drawings of the zipper balun. Drawings of the balun cross sections are provided in Figure 2.1. These were spread out over an eight-inch length, so each cross section is separated by two inches. The center conductor is a round cylinder with diameter 3 cm (1.181 in).

Let us now consider how the zipper fit between the pulser and antenna. Drawings of how the balun fits between the pulser and antenna are in Figures 2.2-2.4. The impedance tapered from 8Ω at the output of H3 to 20Ω at the beginning of the zipper, and then to 50Ω at the end of the zipper. At the end of the oil box, there is a lens and a Brewster window, through which the field is passed that converts the antenna to free space [3].

There are two principles of operation at work in this zipper configuration. First, we wanted to keep the peak field on the center conductor below a maximum value, which we estimated to be 2 MV/cm (in oil) at all points along the center conductor. It was shown using the finite element method in [1] that along the length of the zipper, the field is never any larger than the field at the center of the coaxial feed section. This makes it easy to provide an upper bound on the electric field at any point along the line. Thus, the peak field is the field on the center conductor of the feed coax. From [1, eqn. 4.2], this is just

$$E_{\max} = \frac{V_o}{a \ln(b/a)} \quad (2.1)$$

where a and b are the inner and outer radii of the coaxial feed, and V_o is the peak voltage output of the pulser. Using the values $a = 1.5$ cm, $b = 2.54$ cm, and $V_o = 1$ MV, we find a peak field of 1.3 MV/cm. Thus, we are well within our previously stated specifications.

Let us consider now how we arrived at the conclusion that we wanted to keep the peak electric field below 2 MV/cm. In [4], J. C. Martin gives the rule that breakdown of oil occurs when

$$F^{3/2} t = k \quad (2.2)$$

where F is the average field in a gap, in MV/cm, t is the pulse duration in μs , and k is a constant equal to 0.08 for transformer oil. For an average field of 2 MV/cm and a pulse duration of $0.002 \mu\text{s} = 2$ ns, we find $F^{3/2} t = .005$, which is well below the value of .08 provided by Martin.

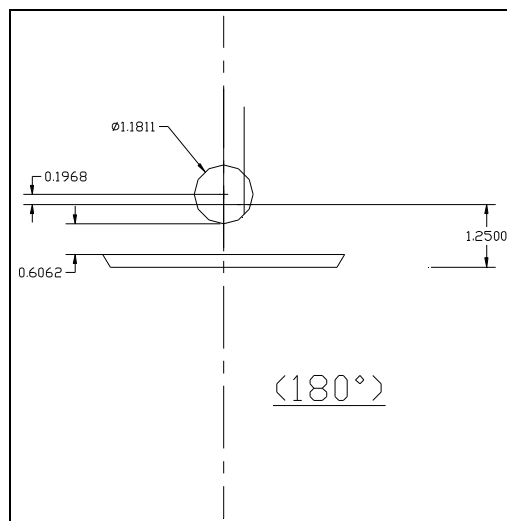
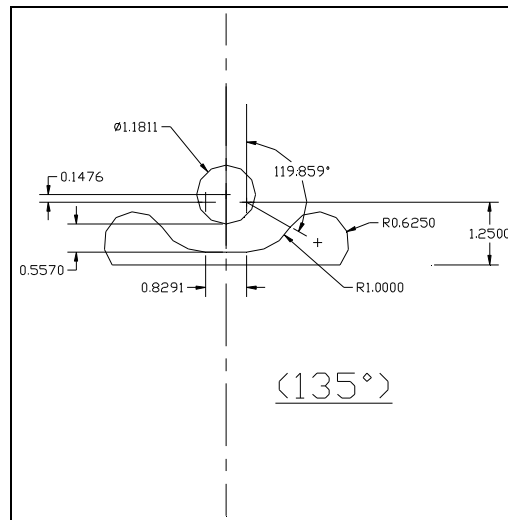
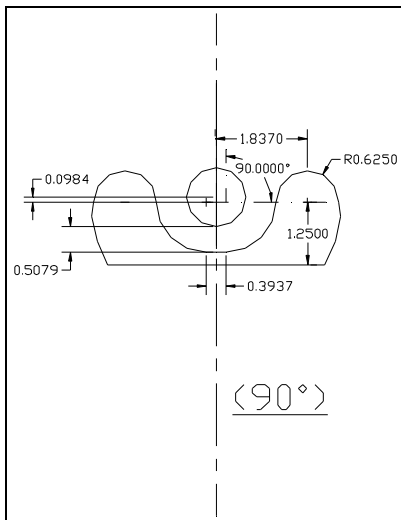
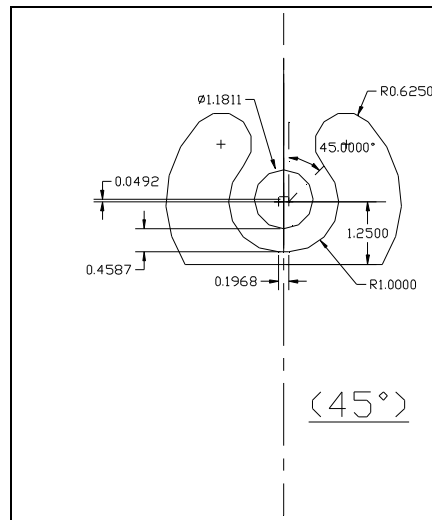
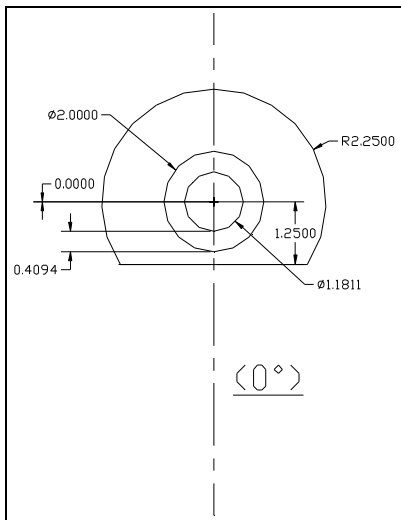


Figure 2.1. Balun zipper at five cuts along the cross section. Units shown are inches.

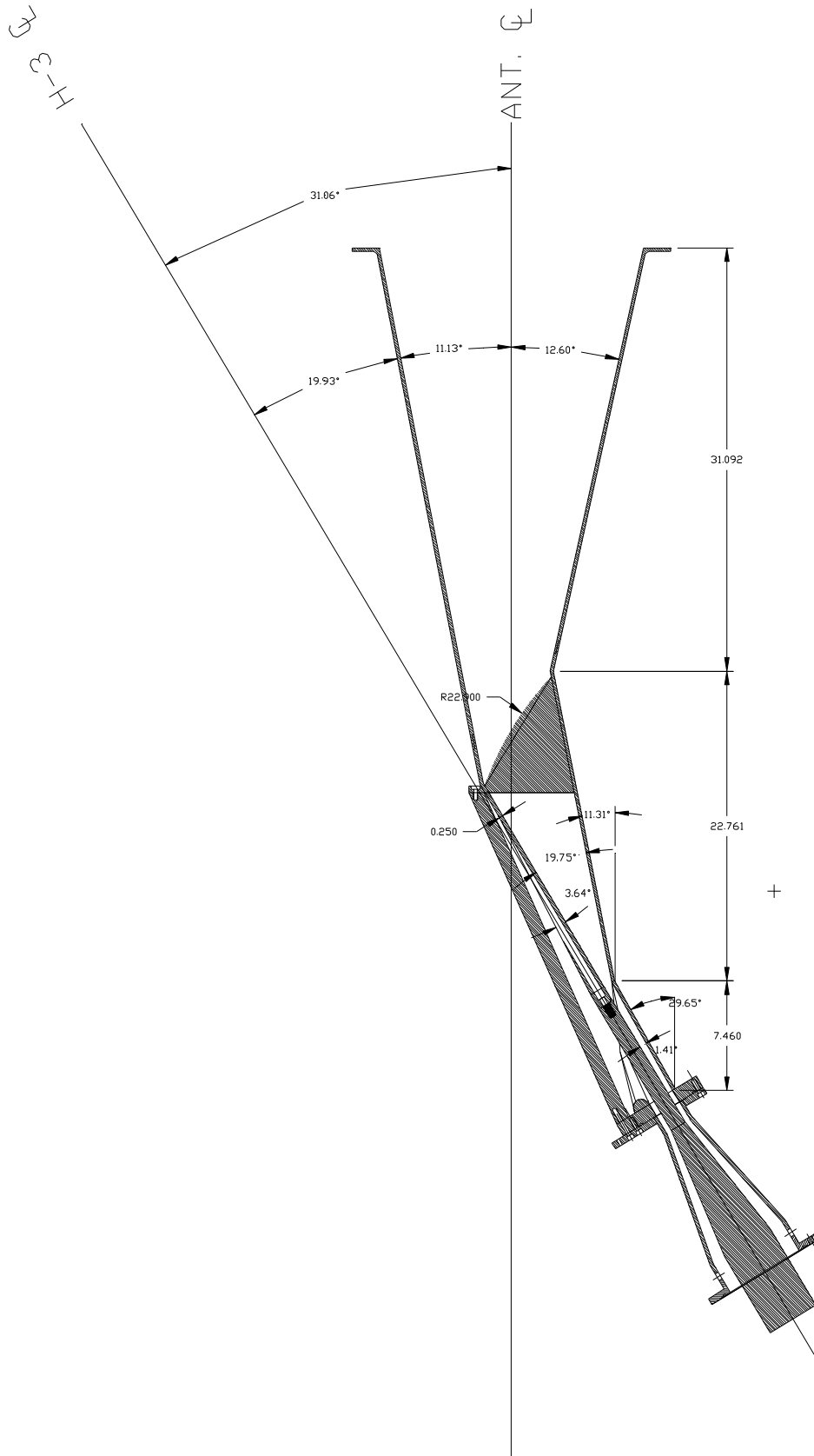


Figure 2.2. The balun and antenna. side view.

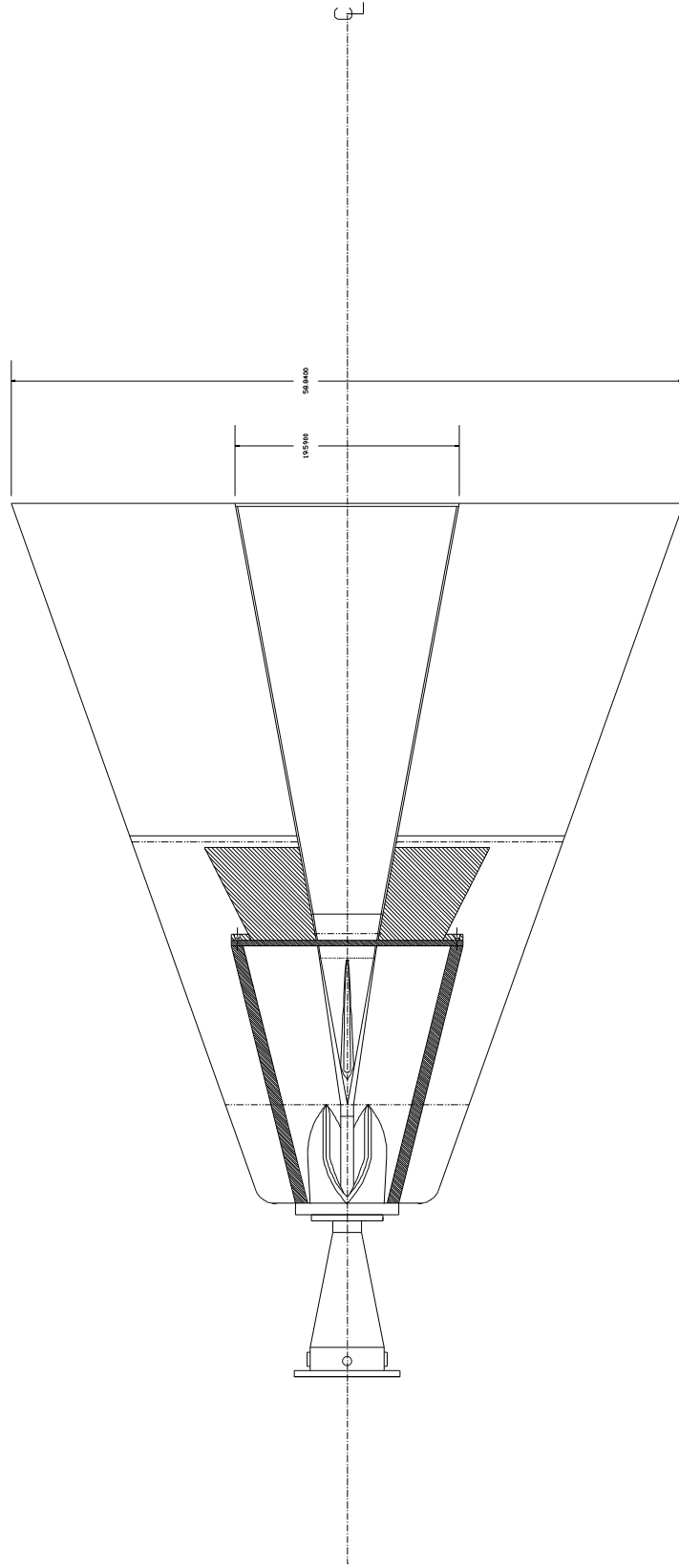


Figure 2.3. Top View of the balun and antenna.

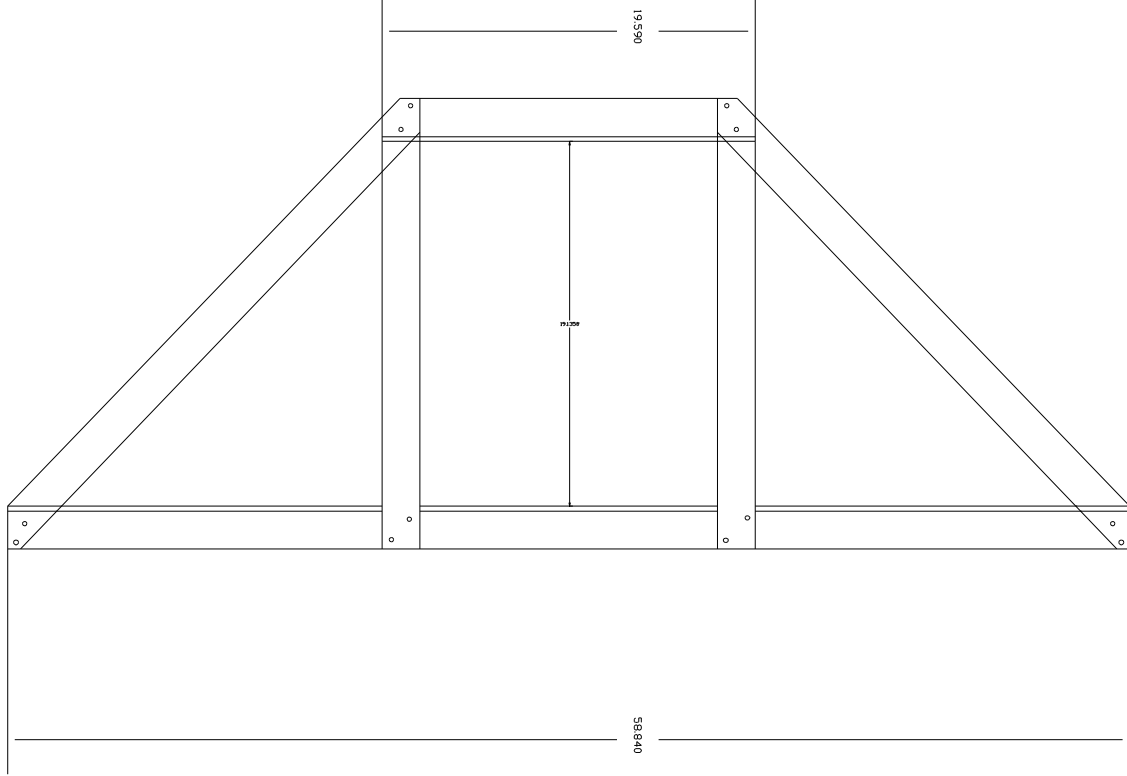


Figure 2.4. Front view of the TEM horn.

Next, we consider the dispersion along the length of the zipper. This is the difference in path lengths between the a ray that travels straight through the zipper, and a ray that follows the longest possible path along the outside of the zipper. It was shown in [1, eqn 6.3] that an upper bound on the time difference is

$$t_{delay} \cong \frac{\sqrt{\epsilon_r} \pi^2 b^2}{2 \ell c} \quad (2.3)$$

where b is the outer radius, ℓ is the transition length, ϵ_r is the dielectric constant, and c is the speed of light in air. Using the numbers $\epsilon_r = 2.2$, $b = 2.54$ cm, and $\ell = 20.32$ cm, we find the dispersion is equal to 77 ps. If, for example, the source waveform was expected to have a risetime of 250 ps, this dispersion would be small compared to the risetime. We can estimate the risetime at the output by adding the risetime of the source in quadrature with the dispersion, and we obtain 262 ps. So once again, we are within our specifications.

Finally, we note that our diagrams of the antenna have left out the resistors. Two strings of Dale NS-10 resistors were placed on either side of the aperture, extending from the top plate to the bottom plate. The resistor values were chosen so they would provide a low-frequency match to the same impedance as the TEM horn, 120Ω . A better approach would have been to feed the resistors from the top plate back to the outer conductor of the feed coax, as described in [5,6]

Having provided the basis for the design, we now consider low-voltage measurements.

III. Low-Voltage Balun Measurements in Air Without Oil or Antenna

We begin now with measurements of the coaxial zipper in air. We performed this measurement as a preliminary measurement before immersing it in oil, which is somewhat more difficult to implement.

The test configuration is fed at the source end by standard $50\ \Omega$ cable into a conical $30\ \Omega$ expansion section. This configuration is shown in Figure 3.1. The straight section is $30\ \Omega$, since there is no oil (it would be $20\ \Omega$ in oil). A TDR is taken with the Tektronix 11801B digital sampling oscilloscope, using the built-in pulser in the SD-24 sampling head. The instrumentation for this configuration is shown in Figure 3.2.

Data from the TDR measurement is shown in Figure 3.3. The zipper shows a smooth transition from $30\ \Omega$ to $70\ \Omega$ in air. In oil, this corresponds to a smooth transition from $20\ \Omega$ to $47\ \Omega$. We had originally intended that the impedance transition to $50\ \Omega$, so we are close to our targeted impedance at the far end.

Next, we measured the fields before and after the zipper. The configuration is shown in Figure 3.4. It consists of a PSPL 4600A pulser, with risetime $71\ \text{ps}$, driving the balun at one end, and with sensor locations after the zipper. Sensors consisted of a bulkhead SMA connector with center conductor extended through the conductor by $2.54\ \text{mm}$ ($0.1\ \text{in}$). These sensors detect the derivative of the field.

The raw data for the measured fields just before and after the zipper are shown in Figure 3.5. The FWHM of the waveforms before and after the zipper are $63\ \text{ps}$ and $80\ \text{ps}$, respectively. If we subtract these two numbers in quadrature, we obtain an impulse response for the zipper of $49\ \text{ps}$ FWHM. Recall that in the previous section we estimated that this zipper would introduce $77\ \text{ps}$ of dispersion into the system. So we have actually introduced less dispersion than we had originally projected, assuming addition of risetimes in quadrature is valid.

Finally, we can take the ratio of the output and input waveforms in the frequency domain. This gives us an idea of how high in frequency the balun is effective. The result is shown in Figure 3.6. We see here that the balun is effective up to about $8\ \text{GHz}$, after which it begins to roll off at the high end.

Having provided data in air, we now immerse the balun in oil and provide measurements with the antenna and lens attached.

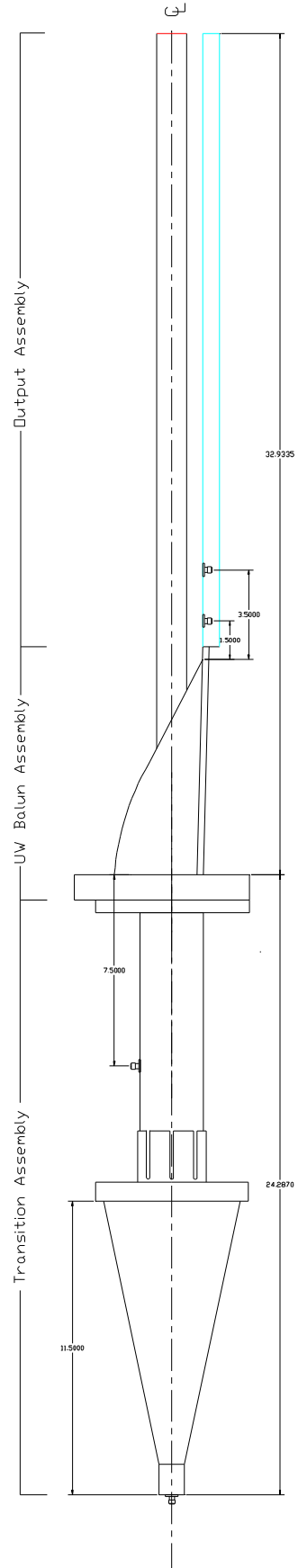
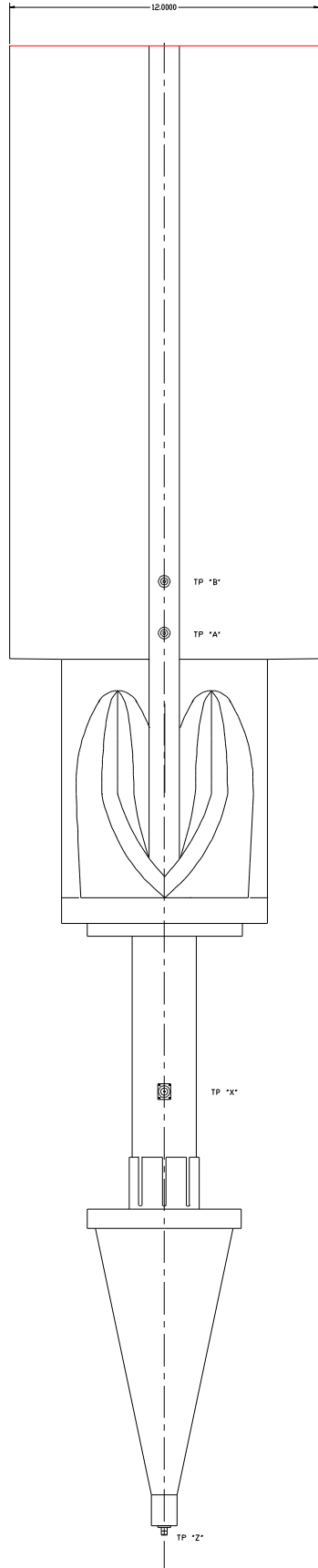


Figure 3.1. Preliminary Balun test in air.

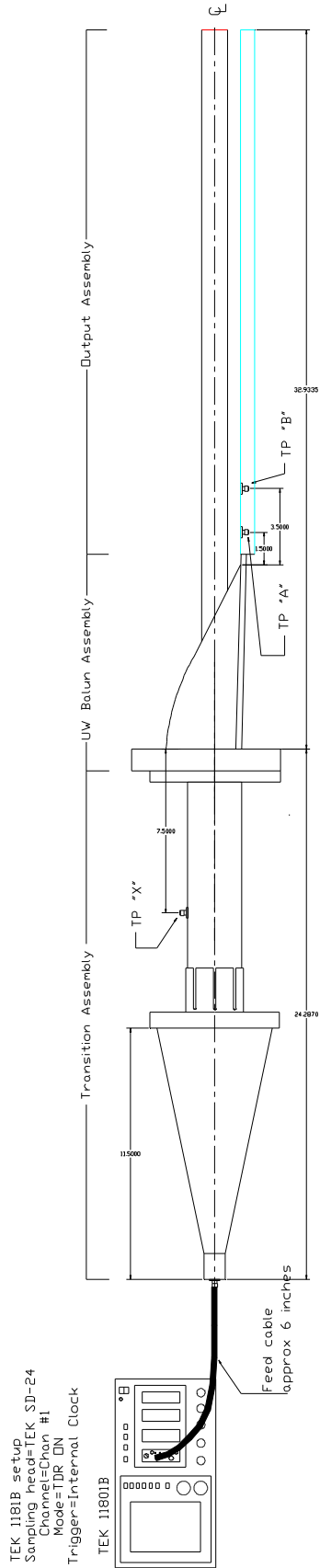


Figure 3.2. TDR Balun test in air.

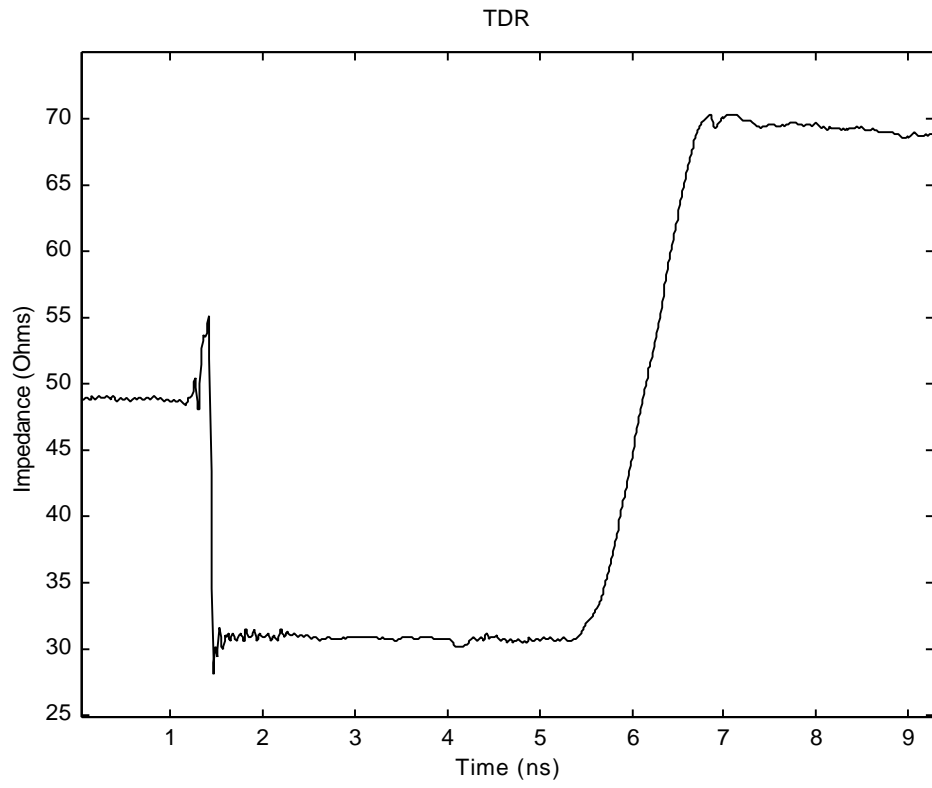


Figure 3.3. TDR of the zipper in air.

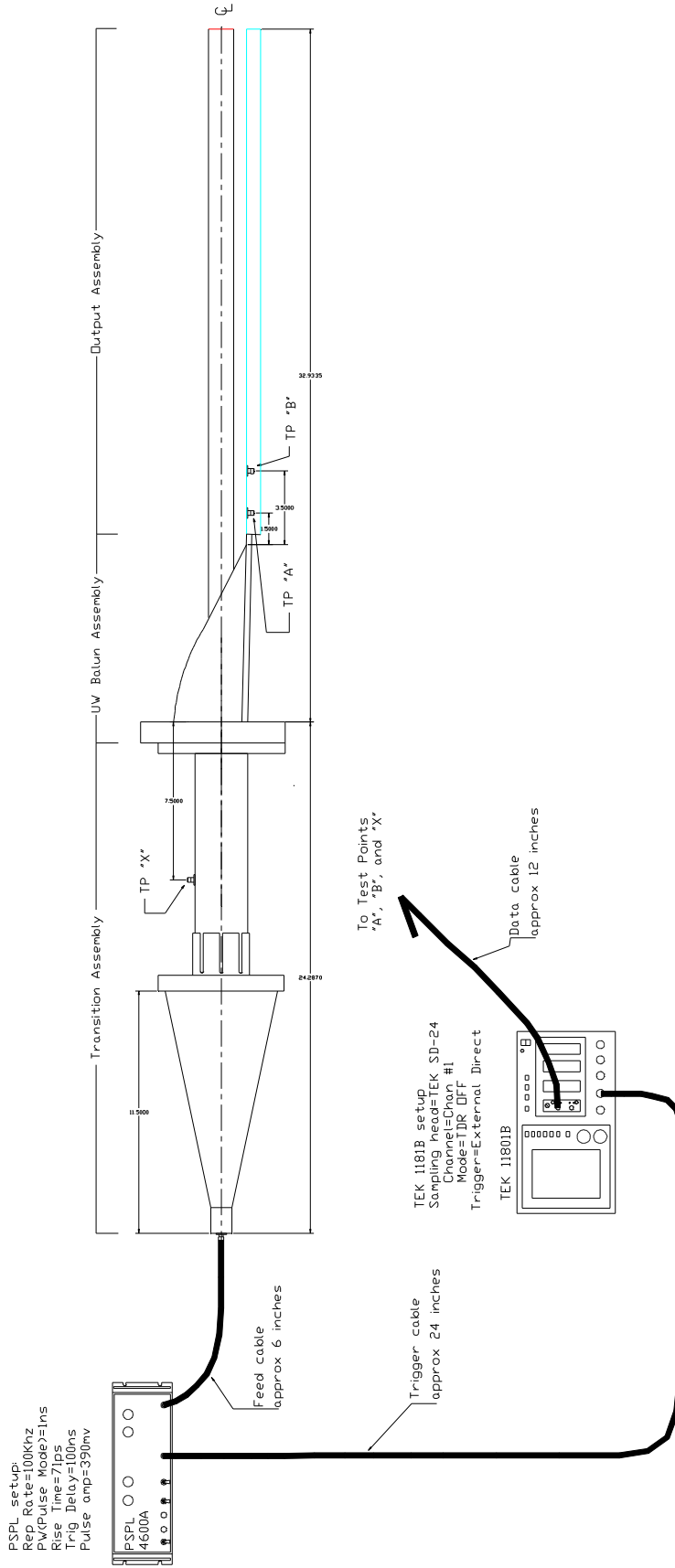


Figure 3.4. Balun transmission test in air.

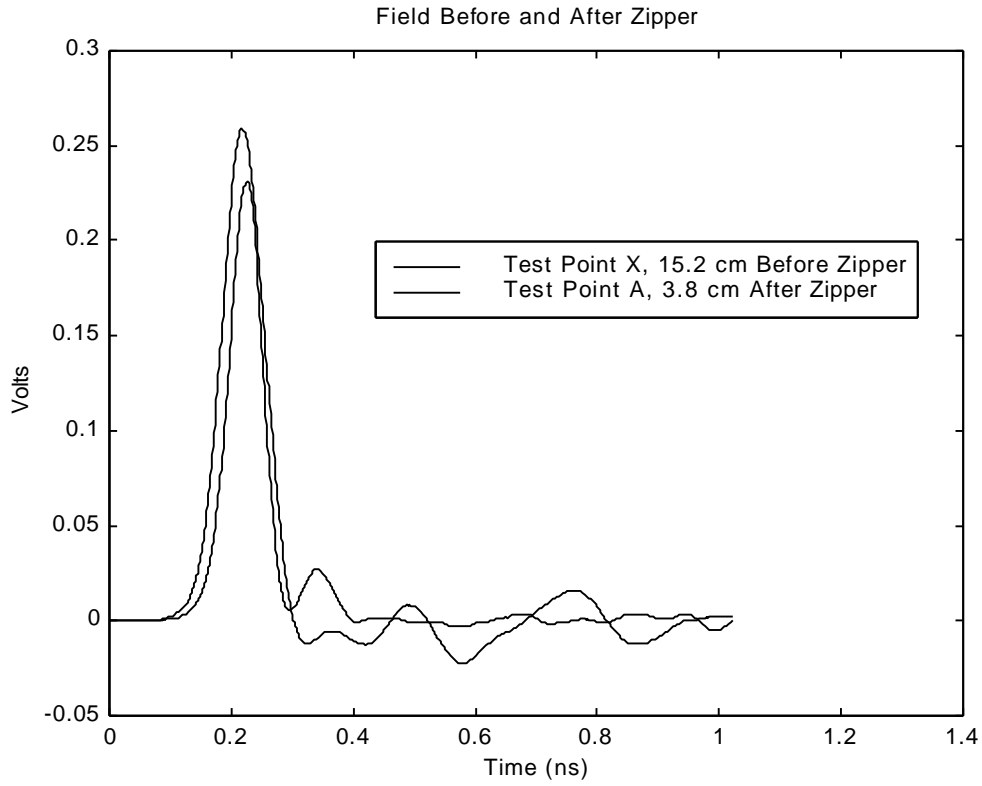


Figure 3.5. Measured fields at test point locations X and A, before and after the zipper.

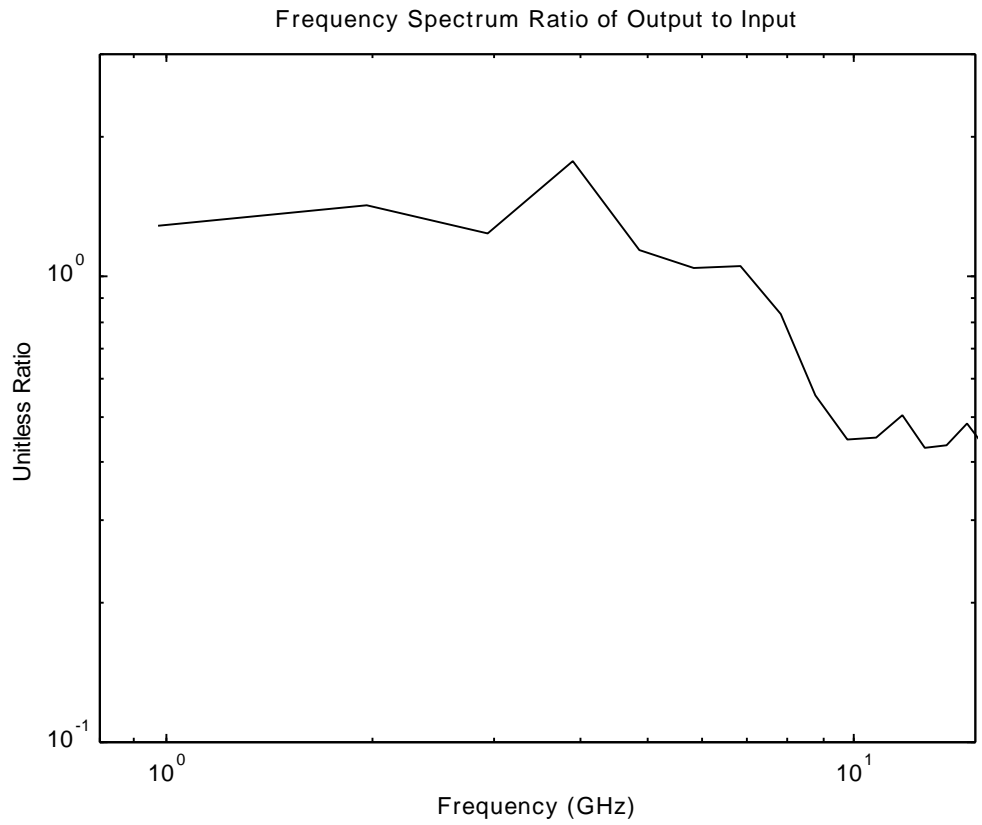


Figure 3.6. Frequency domain ratio of the output and input waveforms.

IV. Measurements in Oil With the Antenna

We next consider measurements that were taken with the zipper in the oil box, and with the lens and TEM horn attached. We made several attempts to provide measurements using the H3 pulser, but we were unable to get data with H3. Therefore, we built an adapter that would allow us to take low-voltage data, driving it instead with a Picosecond Pulse Lab 2600, 40 V step with a risetime of around 350 ns.

First, we provide a TDR of the overall system. A sketch of the experimental setup is shown in Figure 4.1. For a source, we used just the 0.25 Volt source built into the SD-24 sampling head of the Tektronix 11801B. The data is shown in Figure 4.2. We can see the 50 Ω cabling at the beginning, and an abrupt transition to the 20 Ω output feed section. Then there is a gradual transition from 20 to 50 Ohms, due to the zipper. There is a sudden jump up to 60 Ω when the ground plane is bent to begin the conductor separation for the TEM horn. The impedance then increases out along the length of the antenna.

Next, we provide data on the PSPL 2600 source, including the cabling that was used to connect it to the pulser. The measured data is shown in Figure 4.3. The source is a step waveform with risetime of about 350 ps.

Using PSPL 2600 source, we now measure the field at three test points along the length of the balun. The location of the sensors and test setup is shown in Figure 4.4. Sensor #1 is located close to the source. Test point #2 is located after the zipper in the oil box, and test point #3 is located outside the oil box.

A list of the sensors used is provided in Table 4.1, along with their calibration factors. These sensors were provided to us by Voss Scientific. It was observed that the top of the sensors sits about 1.5 mm (0.060 in) below flush with the conductor, so the calibration factors are probably off somewhat.

The data for each of the three sensors is shown in Figures 4.5 through 4.7. Note that this is raw data, and has not been compensated for the source and cables. At sensor #1, we can see a reflection from the zipper occurring between 6 and 8 ns, due to the change in impedance at the zipper.

Next, we provide radiated field measurements. The test configuration is shown in Figure 4.8. We used a free-field E-dot sensor (Prodyne AD-70(R)) with a balun (Prodyne BIB-100F) to make the measurement 1.0 meter in front of the TEM horn. The raw derivative voltage data is shown in Figures 4.9. At one meter distance, we are seeing the second derivative of the driving voltage. Note that one derivative is introduced by the sensor, and one derivative is introduced by the antenna, which is expected to radiate the derivative of the driving voltage.

Next, we wish to convert the raw measured voltage to an electric field. To do so, we must recognize that what we are measuring with our D-dot sensor is

$$V(t) = K_{bal} R A_{eq} \epsilon_o \frac{dE(t)}{dt} \quad (4.1)$$

This is a slightly modified version of the formula for the measured voltage of a D-dot sensor. The modification is the attenuation factor, K_{bal} , which just represents the attenuation of the signal through the Prodyne balun. For our sensor, $R = 100 \Omega$, $A_{eq} = 10^{-3} \text{ m}^2$, and $\epsilon_o = 8.854 \times 10^{-12} \text{ F/m}$. Furthermore, the manufacturer specifies that the loss through the balun is 8 dB, so $K_{bal} = 0.4$. We can now invert the above equation to obtain the measured electric field as

$$E(t) = \frac{1}{K_{bal} R A_{eq} \epsilon_o} \int_0^t V(t) dt \quad (4.2)$$

Note that both the sensor and balun calibrations can in general have some frequency dependence, but we have assumed that we are operating in a linear regime. The integrated field data is shown in Figure 4.10. We see at a 1 meter distance from the aperture a peak electric field of 34 V/m, using the PSPL 2600 source. Note that the antenna aperture is 1.1 meters from the phase center of the antenna, so the sensor located at 1 meter in front of the aperture is actually 2.1 meters from the phase center.

Let us consider now how to scale the above result to parameters that are more typical of high-voltage parameters. Assume that we wish to know the field at 100 m distance, when the voltage at the 20 Ω input section is 1 MV. The field is directly proportional to the voltage, and inversely proportional to the distance. So the measured field of 34 V/m will scale by factors of $(10^6/38)$ in voltage and $(2.1/100)$ in distance. This leads to an estimate of 19 kV/m at 100 m.

The above estimate requires a number of qualifications. First, we have assumed that the risetime of 350 ps remains the same in the high-voltage version. If the high-voltage pulse is faster, then the radiated field becomes faster by the ratio of risetimes. Second, we have assumed that the sensor is in the far field at a one-meter distance from the antenna aperture. It is only in the far field that the magnitude is inversely proportional to distance. However, note that if the sensor really was in the near field, then our estimate would be on the low side of the actual number.

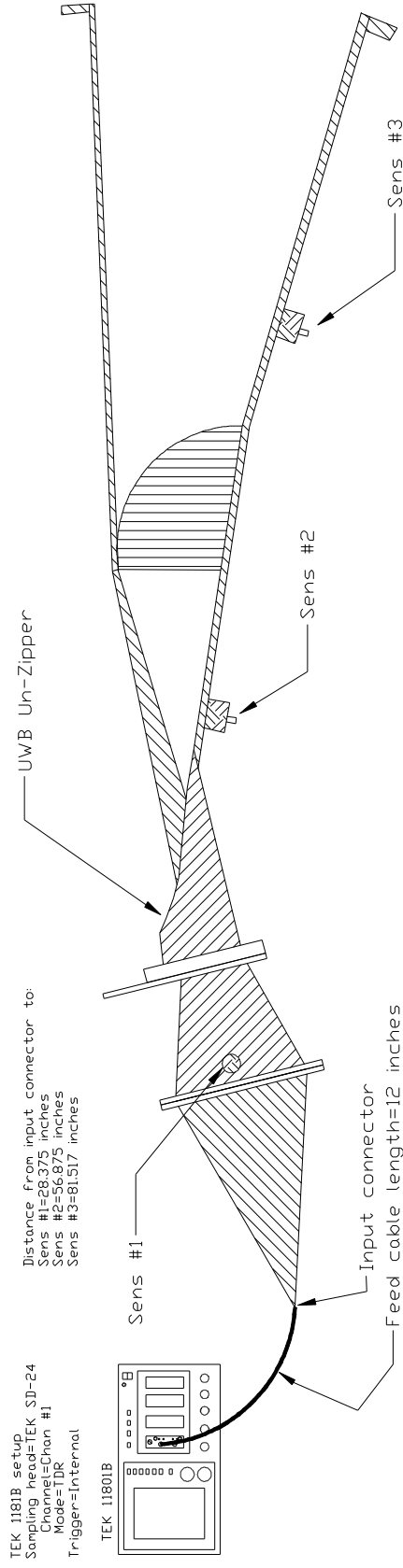


Figure 4.1. Balun TDR measurement with oil and antenna.

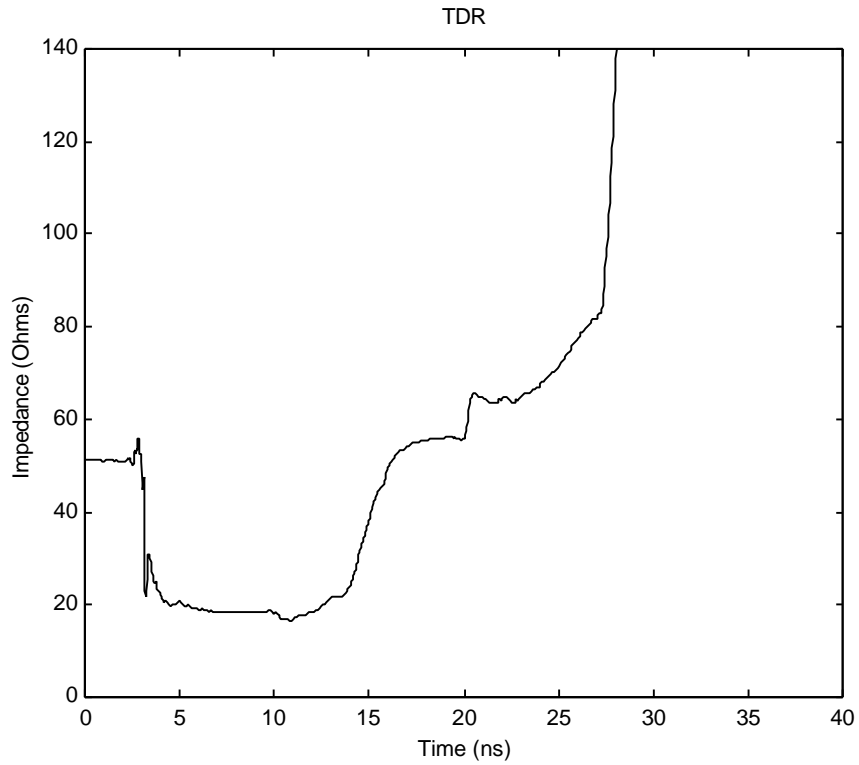


Figure 4.2. TDR Data of balun with oil and antenna.

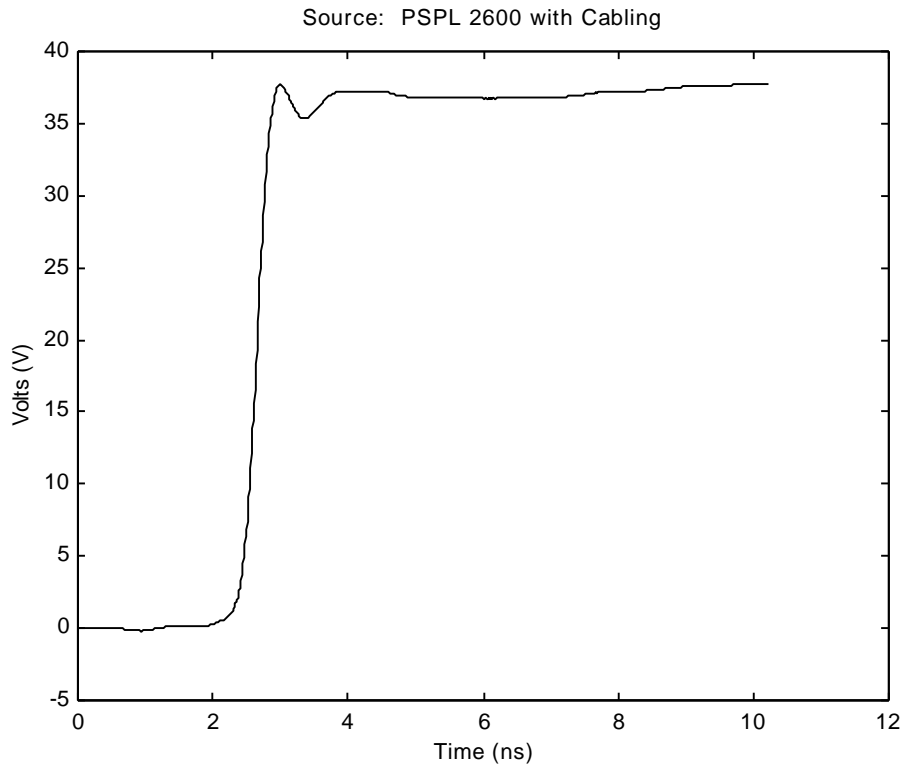


Figure 4.3. The step source waveform, PSPL 2600 with cabling.

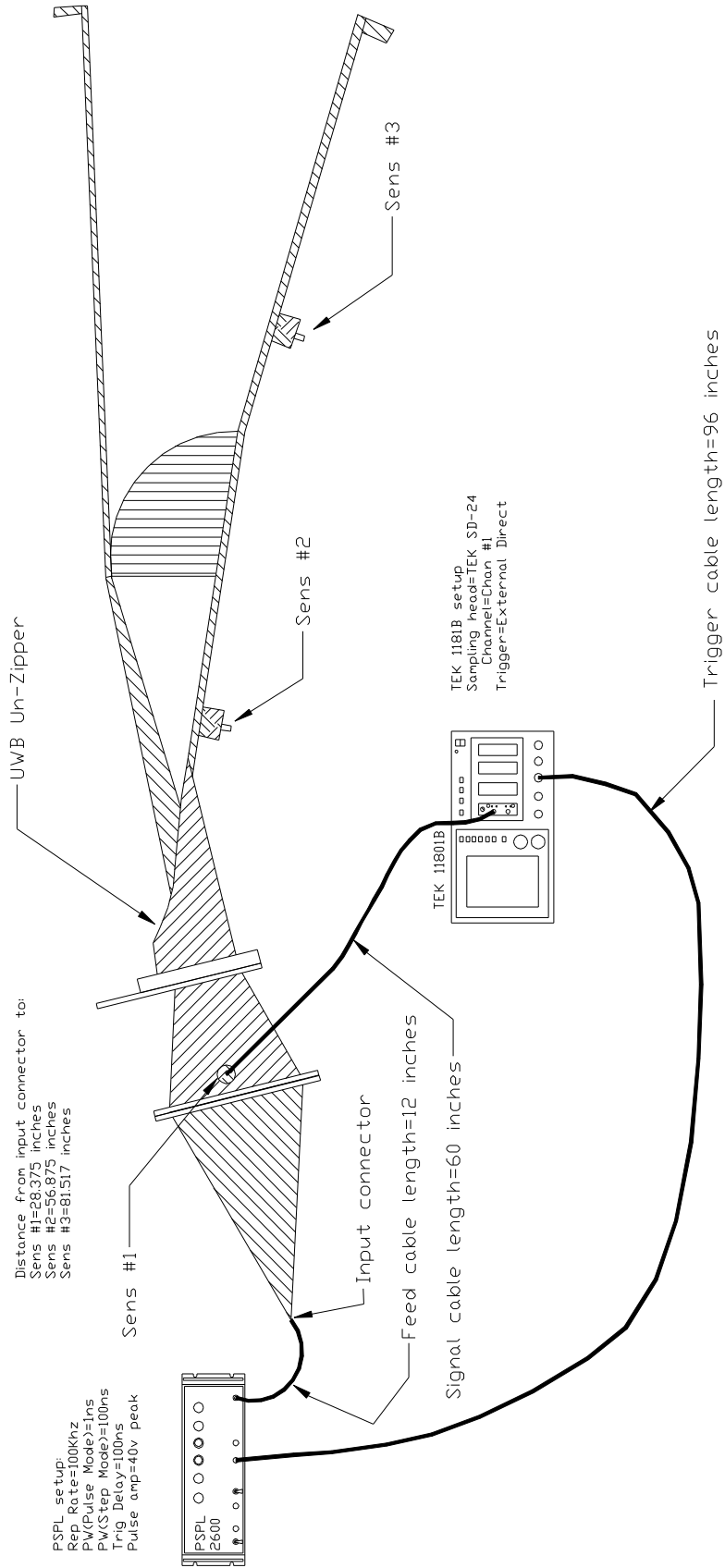


Figure 4.4. Balun field measurement at various points along the antenna and feed.

Table 4.1. Self-Integrating E-field (SIE) Sensors

Location	Sensor	Calibration Factor (m)
1	F104/F6	6.15×10^{-6}
2	F111/M2	7.72×10^{-6}
3	F106/M5	7.8×10^{-6}

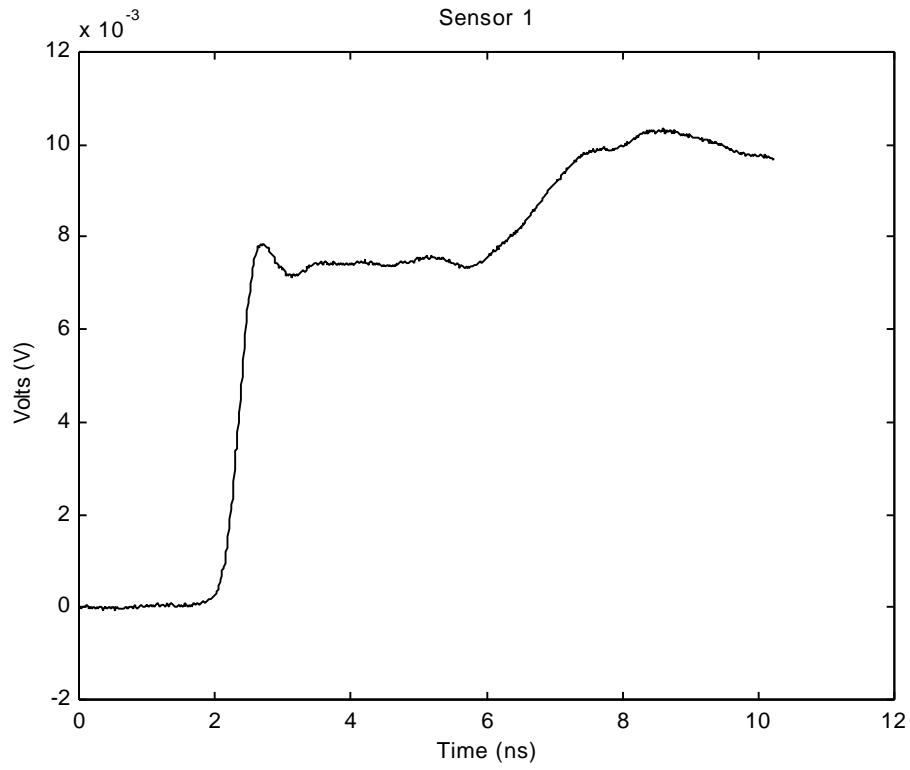


Figure 4.5. Measured step response at Sensor #1.

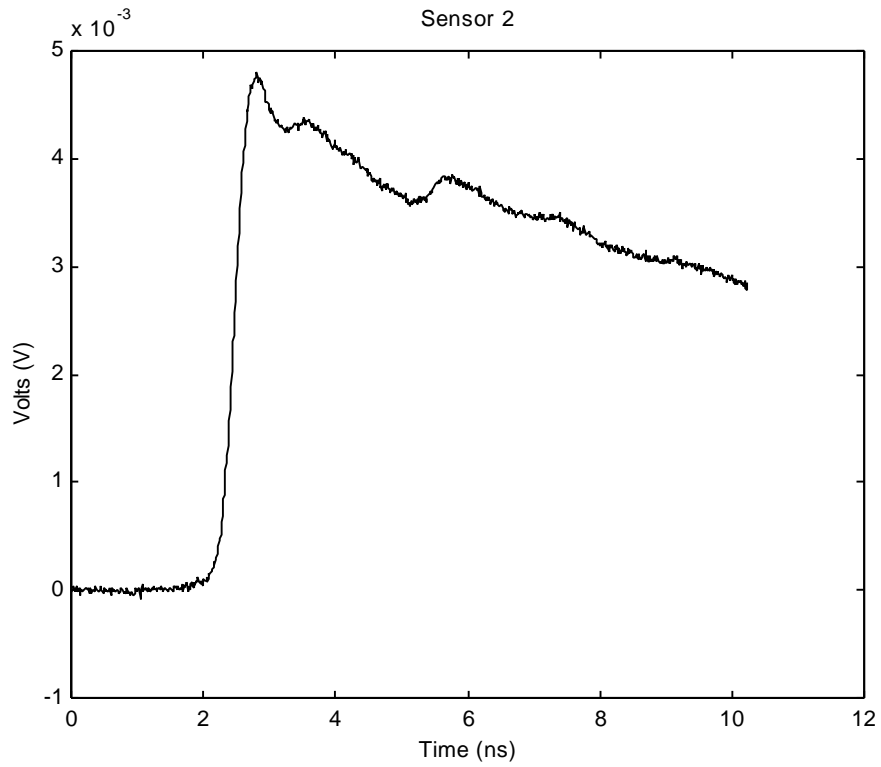


Figure 4.6. Measured step response at Sensor #2.

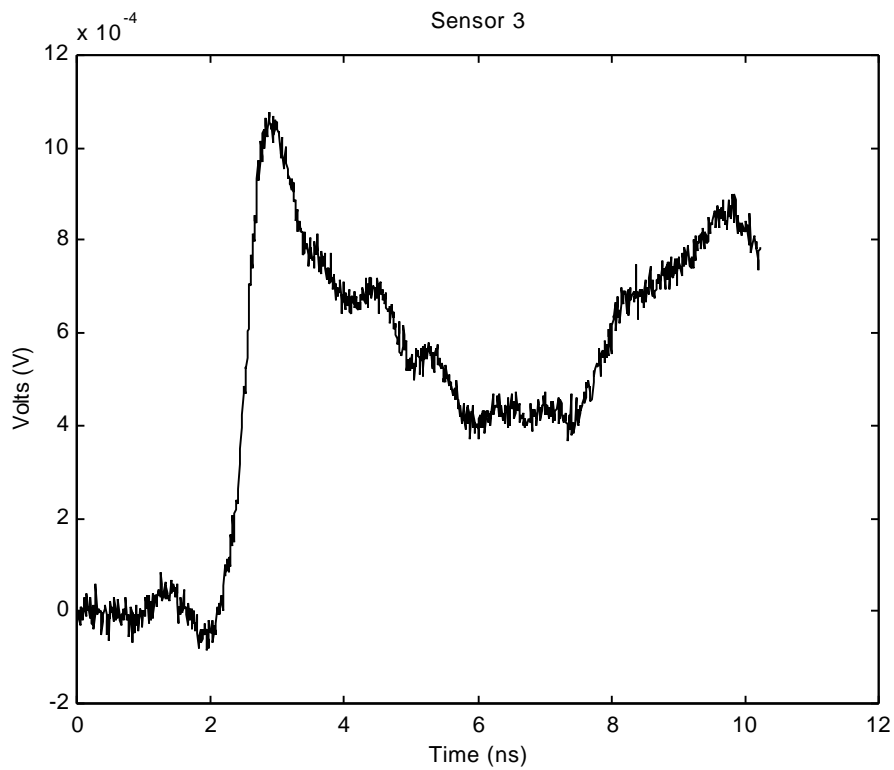


Figure 4.7. Measured step response at Sensor #3.

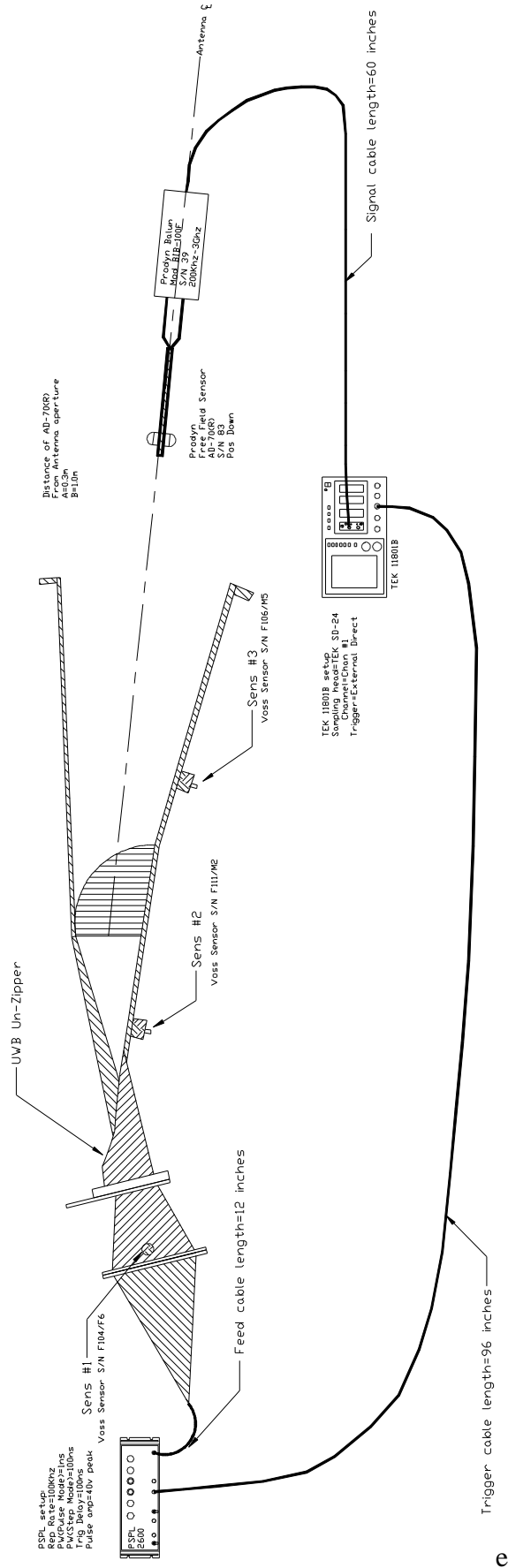


Figure 4.8. Configuration for field measurement in front of the antenna.

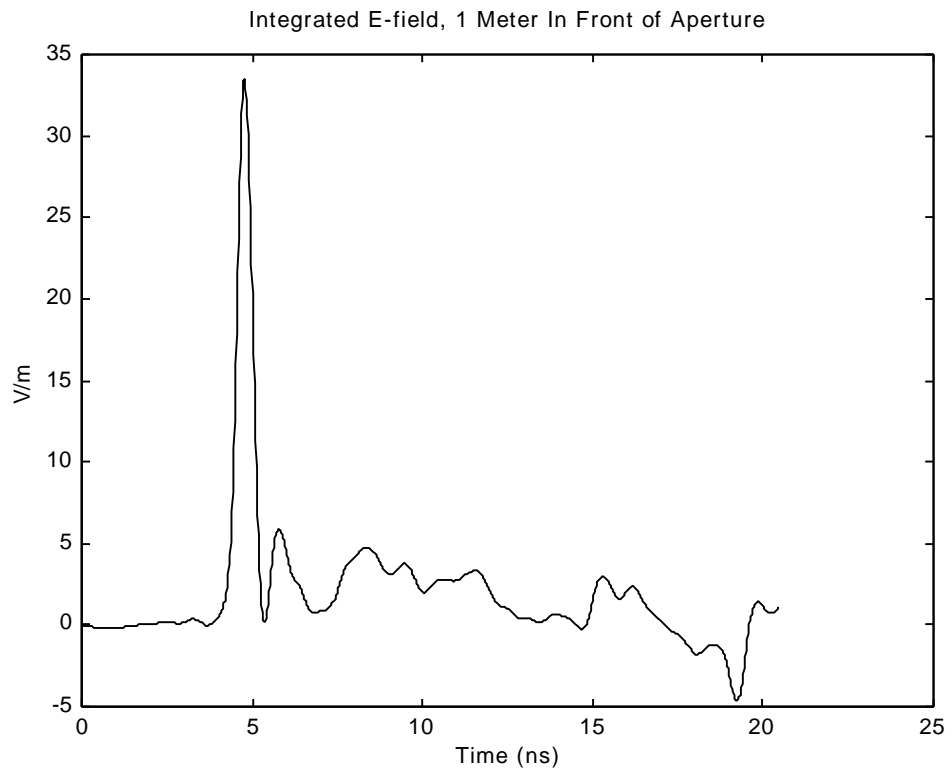
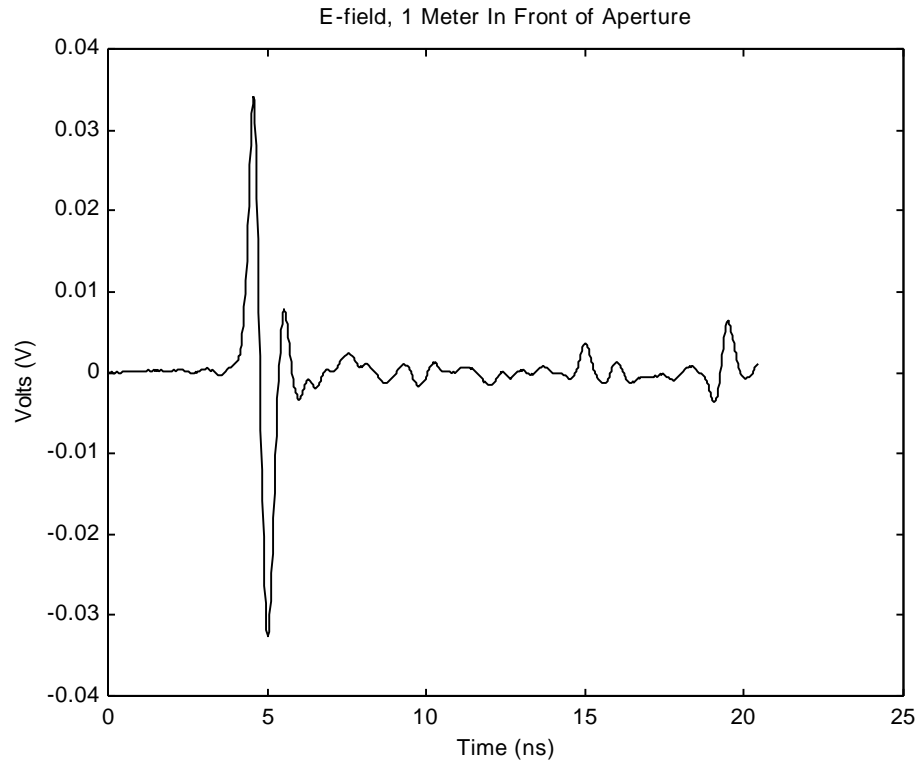


Figure 4.9 Field measurement 1 meter in front of the aperture, raw data (top) and integrated and scaled (bottom).

V. Discussion

Having built and tested the balun and antenna, we now consider how it might be modified or improved in any future versions.

First, we consider changes in the electrical design. In this design we chose a set of design parameters that might have been better suited to higher fields and faster risetimes than what is provided by the H3. In order to keep the dispersion to a minimum, one wants to have as small a diameter coaxial zipper as possible. To do this, while passing as much energy as possible without breaking down, we found in [1] that the optimal impedance is 20Ω . That was why we chose to start our zipper at an impedance at 20Ω , but this forced us to postpone tapering our impedance for a long time, and then the taper from 20Ω to 50Ω occurred rather suddenly. A more gradual taper would have generated less reflections from the zipper. We believe that we are well within specifications for both high-voltage breakdown and dispersion within the zipper. Thus, we could relax our design in these areas with little effect, and get somewhat better performance from the H3 by using a more gradual taper.

We have claimed above that we are well within specifications for electric field breakdown and dispersion in the zipper for H3. However, since we have not yet actually tested the device at higher voltages, this is still based only on engineering judgement. It would be far better to test the device at higher voltages.

Finally, we consider logistical changes in the design. We found it to be a bit clumsy to use RTV to seal the oil box each time we wanted to adjust the inner workings of the zipper. This required a several-day cycle each time we opened up the balun to make any adjustments, due to a requirement to let the RTV set, and then test for leaks. In the future, an O-ring seal should be considered.

VI. Concluding Remarks

We have built and tested a coaxial zipper at low voltages. Using a variety of low-voltage measurements we have shown that the zipper is effective as high as 8 GHz, and we have estimated the radiated fields at larger distances and higher voltages.

The work that remains to be done is to test the device at higher voltages and at larger distances. It is hoped that this can be done soon.

Acknowledgements

We wish to thank William D. Prather of Air Force Research Laboratory / DEHP for funding this work.

References

- [1] E. G. Farr, G. D. Sower, and C. J. Buchenauer, Design Consideration for Ultra-Wideband, High-Voltage Baluns, Sensor and Simulation Note 371, October 1994.
- [2] G. D. Sower, L. M. Atchley, D. E. Ellibee, and E. G. Farr, Low-Voltage Prototype Development of an Ultra-Wideband High-Voltage Unzipper Balun, Measurement Note 50, December 1996.
- [3] C. E. Baum, Brewster-Angle Interface Between Flat-Plate Conical Transmission Lines, Sensor and Simulation Note 389, November 1995.
- [4] J. C. Martin, Comparison of Breakdown Voltages for Various Liquids Under One Set of Conditions, Dielectric Strength Note 1, November 1965. Also appears as pp. 177-179 in *J.C. Martin on Pulsed Power*, edited by T. H. Martin, A. H. Guenther, and M. Kristiansen, Plenum Press, 1996.
- [5] M. H. Vogel, Design of the Low-Frequency Compensation of an Extreme-Bandwidth TEM Horn and Lens IRA, Sensor and Simulation Note 391 (with corrections), April 1996.
- [6] C. E. Baum, Low-Frequency Compensated TEM Horn, Sensor and Simulation Note 377, January 1995.